Research Article

Use of organo-montmorillonite for the nitrate retention in water: influence of alkyl length of loaded surfactants

Maria A. Jaworski[1,2] · Federico M. Flores[3] · Mariela A. Fernández[3] · Mónica Casella[1] · Rosa M. Torres Sánchez[3]

Abstract
The removal of NO_3^- from water was performed and compared among four organo-montmorillonites (OMt) with quaternary amine surfactants of different chain lengths [octadecyl trimethyl-(ODTMA), hexadecyl trimethyl-(HDTMA), tetradecyl trimethyl-(TDTMA) and dodecyl trimethyl-ammonium (DDTMA)] and loadings [100%, 200%, 400% of the Mt cation exchange capacity (CEC)]. The maximum adsorption of NO_3^- was attained by the long chain length surfactants (64 and 100 mg NO_3^- ions per gram of OMt, for HDTMA and ODTMA, respectively) with initial loading of 400% with respect to the CEC of Mt. The short chain length surfactants (DDTMA and TDTMA) did not show adsorption of NO_3^- except for TDTMA 400 sample. The NO_3^- adsorption produced a slight expansion of the interlayer thickness of the OMt samples loaded with long-chain surfactants that was assigned to the entrance of NO_3^- by a synergic effect with these surfactants. The decrease of the negative zeta potential, found for OMt samples relative to that of Mt sample, was attributed to the surfactant chain length rather than to the actual surfactant loaded amounts, which allowed attaining positive zeta potential values for the OMt loaded with long-chain surfactants. The NO_3^- adsorption on OMt samples caused a slight decrease in the positive zeta potential values, reflecting the external surface coating by NO_3^-. For long-chain molecules, this behaviour also indicated the formation of greater interactions such as ion pairs between the positive polar group of the surfactant and NO_3^- ions.

Keywords Organo-montmorillonites · Surfactant alkyl length · Water treatment · Nitrate retention · Synergic effect

1 Introduction

The production of nitrogen fertilizers in large quantities, based on the artificial synthesis of ammonia [1], has allowed their intensive use in soils to improve the agricultural yield. Therefore, NO_3^- concentration has been increasing steadily in groundwater since 1950 [2]. In addition, the elimination of untreated municipal and industrial waste has increased the contamination of water by NO_3^-, generating some serious problems in the quality of water destined to human consumption [3, 4].

The intake of water containing NO_3^- has adverse effects on human health, so maximum tolerable levels have been established for NO_3^- in water for human consumption. The maximum contaminant level allowed by the US Environmental Protection Agency (EPA) is 10 ppm for N–NO_3^- (expressed in terms of nitrogen in NO_3^-) in the water supply for the population [5]. For the World Health Organization (WHO) it is 50 ppm for NO_3^- and 1 ppm for NO_2^- [6].

The NO_3^- is harmful because it is reduced to NO_2^- in the mouth and intestines, favouring the development of methemoglobinemia, which causes a deficiency of oxygen in the blood that can be life-threatening, especially in children under six months of age ("blue baby syndrome"). When NO_3^- is transformed to NO_2^- in the human body,

✉ Maria A. Jaworski, majaworski@quimica.unlp.edu.ar | [1]CINDECA, Facultad de Ciencias Exactas, UNLP - CCT La Plata - CONICET, 47 No. 257, 1900 La Plata, Argentina. [2]Facultad de Ingeniería, Universidad Nacional de La Plata, La Plata, Argentina. [3]CETMIC-CONICET-CCT La Plata-CICPBA, Camino Centenario y 506, 1897 M. B. Gonnet, Argentina.

SN Applied Sciences (2019) 1:1318 | https://doi.org/10.1007/s42452-019-1349-8

Received: 6 August 2019 / Accepted: 24 September 2019 / Published online: 3 October 2019

other reactions can take place. The NO_2^- could react with amine compounds to form the so-called N-nitrosamines (NOC, N-nitrous compound), some of which have proved to be mutagenic and carcinogenic [7].

Due to its high stability and solubility, NO_3^- has a low tendency for precipitation and adsorption and therefore, it is difficult to remove this ion from contaminated water using conventional water treatment technologies [8]. Current technologies for NO_3^- removal, such as ion-exchange and reverse osmosis, are not selective to NO_3^- and also generate secondary waste brine and require frequent media regeneration [9, 10].

The adsorption process involves the adhesion of atoms, ions or molecules from a gas, liquid or dissolved solid to a surface. The absorbents are the materials that present satisfactory results in removing contaminants from water [11]. So, the adsorption process is a suitable technique for inorganic and organic pollutant removal from wastewater having some more significant advantages than other techniques such as low cost, availability, profitability, ease of operation, efficiency, and effectiveness. In particular, for NO_3^- removal from water, different adsorbents have been tested, including natural and synthetic materials, carbon-based adsorbents, originating from agricultural waste and synthetic resins [12–14], compounds similar to hydrotalcite [15], and nanocomposites made of zirconium oxide from chitosan/Y/nano zeolite [4]. The limitation for its technological use is based mainly on the low cost and/or the regeneration of the adsorbent [3, 4]. The use of clays as adsorbents has some advantages compared to other adsorbents in terms of low cost, abundant availability, high specific surface area, and non-toxic nature [16–21]. The high density of negative charges and the presence of exchangeable cations on the surface of the clays make them efficient adsorbents for cationic pollutants [22], causing an opposite effect for anionic contaminants, in particular inorganic anions and oxyanions such as nitrate, chromate and arsenate [23]. Organic surfactants have been used to tailor activated carbon electrodes of high surface area [9, 13, 24, 25] and clays to improve the retention capacity of inorganic anions such as NO_3^- [3, 26, 27]. In addition, bentonite clays have been modified with organic surfactants (quaternary ammonium cations) in order to improve atrazine removal [28]. Among the surfactants used, quaternary amines with different chain lengths and quantities were loaded on raw montmorillonite clay (Mt), to obtain the so-called organo-montmorillonite (OMt) [17–19, 29–32]. The large surface area of these clays allows them to anchor and concentrate a large amount of surfactants on their surface [33]. The first adsorption stage is governed by the cation exchange in the Mt interlayer, until the surfactant concentration equals the value of cation exchange capacity (CEC), and whose arrangement at the interlayer can be followed by X-ray diffraction analysis (XRD) [29]. Higher concentrations of surfactant adsorbed, > 1.0 CEC, produce ion pairs at the outer surface of Mt, modifying the electric surface charge [18, 31, 34].

Since the main mechanism for NO_3^- adsorption is the electrostatic attraction between the protonated amine groups ($-NH_3^+$) at the OMt surface [25, 35], the increase of surfactant content would improve NO_3^- adsorption.

In this work, four different OMt samples, loaded at 100%, 200% and 400% CEC with different chain lengths of quaternary amine surfactants [octadecyl trimethyl-(ODTMA), hexadecyl trimethyl-(HDTMA), tetradecyl trimethyl-(TDTMA) and dodecyl trimethyl-ammonium (DDTMA)] were used for NO_3^- adsorption. The organo-montmorillonite samples and products obtained with maximal NO_3^- retention were characterized by Fourier transform infrared spectroscopy (FTIR), thermogravimetric analysis (TGA), XRD and zeta potential determinations, in order to determine the interactions and surface sites involved.

2 Experimental section

2.1 Materials

Na-montmorillonite (> 99%) [36], labelled as Mt, was provided by Castiglioni Pes and Cia. (Lago Pellegrini deposit, Río Negro, North Patagonia, Argentina) and used as received. The structural formula obtained from the chemical analysis was $[(Si_{3.89}Al_{0.11})(Al_{1.43}Fe^{3+}_{0.28}Mg_{0.30})O_{10}(OH)_2]Na^+_{0.41}$ and its main properties were: isoelectric point (IEP) pH = 2.7, specific surface area (SSA) = 34.0 $m^2 g^{-1}$, total specific surface area (TSSA) = 621 $m^2 g^{-1}$ [36] and CEC = 0.825 mmol g^{-1} [18].

The octadecyl trimethyl-ammonium bromide (ODTMA, ≥ 98%, MW = 392.5 g mol^{-1}, and critical micelle concentration (CMC) = 0.3 mM) was purchased from Fluka (Buchs, Switzerland). The hexadecyl trimethyl-ammonium (HDTMA), tetradecyl trimethyl-ammonium (TDTMA) and dodecyl trimethyl-ammonium (DDTMA) bromides were purchased from Sigma Aldrich Chemical Company Inc. and used as received (98%, 99% and 98% purity, MW = 364.5, 336.41 and 308.34 g mol^{-1} and CMC = 0.1 mM, 0.3 mM and 15.18 mM, respectively.)

All surfactants were used as received.

2.2 Organo-montmorillonite preparation

In the preparation of the OMt at several surfactant loadings, the corresponding concentrations of ODTMA, HDTMA, TDTMA and DDTMA solutions were kept under stirring (200 rpm) for 2 h at 60 °C with 10 g L^{-1} of Mt. For

all the OMt samples, the amounts corresponding to 100%, 200% and 400% with respect to the Mt CEC were used. The products obtained were washed with distilled water three times to remove the surfactant excess. Samples were labelled with the surfactants, and the initial surfactant loading as a percentage of the CEC value (i.e. ODTMA 200, HDTMA 100, etc.).

2.3 NO_3^- adsorption experiment

Adsorption measurements were made by mixing a nitrate solution with the corresponding OMt sample at room temperature. About 0.1 g of OMt was placed in a 100 mL glass bottle containing 50 mL of anion solution at 100 mg L^{-1}, pH 5.4. Solutions were under continuous stirring for 24 h. The measurements were performed in duplicate.

After the contact time, the suspensions were centrifuged at 3000 rpm for 15 min. The supernatant was analysed by ion chromatography (*Metrohm 790 Personal IC*) to determine NO_3^- concentration. A solution of $NaHCO_3$ 1.0 mM and Na_2CO_3 3.2 mM was used as the mobile phase, the flow rate was set at 7 mL min^{-1}.

The amount of adsorbed NO_3^-, Q_{ADS}, (mg NO_3^- g^{-1} clay) was determined as the difference between the initial NO_3^- concentration (C_i) and after contact time (C_e).

2.4 Characterization methods

TGA experiments were conducted using a NETZSCH STA 409 PC/PG with alumina as a reference. Samples of 20 mg were placed in alumina crucibles and heated from 30 to 800 °C at a scanning rate of 10 °C min^{-1} in air atmosphere. The actual surfactant loading for all OMt samples was obtained by calculation from the mass loss values in the temperature range from 150 to 800 °C, taking into account the mass loss of Mt structural hydroxyl groups [37].

FTIR was performed for all powder samples in KBr discs (1 mg of sample and 100 mg KBr). The FTIR spectra were recorded by accumulating 64 scans over the 4000–400 cm^{-1} region at a resolution of 4 cm^{-1} using Nicolet iS10 (Thermo Fisher Scientific, USA) equipment.

XRD patterns were recorded on oriented samples, in the range $2° < 2\theta < 30°$, with a counting time of 10 s $step^{-1}$, 0.02° (2θ) step size, 40 kV and 30 mA with Cu K_a radiation using a Philips PW 1710 diffractometer.

Electrokinetic potentials were determined using Brookhaven 90Plus/Bi-MAS. The electrophoretic mobility was converted automatically into zeta potential values using the Smoluchowski equation. To generate zeta potential versus pH curves, 40 mg of sample was dispersed in 40 mL KCl 1 mM, used as inert electrolyte. The slurry was continuously stirred and the suspension pH was adjusted adding HCl or KOH.

3 Results and discussion

3.1 NO_3^- retention experiment

The results of NO_3^- adsorption in Mt and all OMt samples are shown in Fig. 1a. The negligible NO_3^- adsorption found for Mt sample was in agreement with results reported for untreated clays (smectite, kaolinite and halloysite by Xi et al. (2010). Although the adsorption of NO_3^- is related to the increase of positive charges on the OMt surface, provided by the ammonium charged head of the surfactant [3], different effects are depicted in Fig. 1a according to the chain length of the surfactant used. While OMt samples modified with short-chain surfactants (samples loaded with DDTMA and TDTMA) showed no adsorption of NO_3^-, except for TDTMA400, a general increase in NO_3^- uptake appeared for OMt samples loaded with long-chain surfactants (HDTMA and ODTMA). In addition, these last samples reached maximum retention values of NO_3^- (100 and 64 mg NO_3^- per gram of OMt), for the samples with the highest content of the corresponding surfactant (ODTMA400 and HDTMA400, respectively) (Fig. 1a).

The different behaviour in NO_3^- retention shown by short- or long-chain surfactant loaded OMt suggested that the surfactants could be attached preferentially to different surface sites of the Mt, and/or a different actual amount was attained among the different chain lengths of surfactants employed.

In further sections it was determined (Table 1) that the actual surfactant content, corresponding to the initial CEC load, varies from 67.9 to 379.5% CEC (from DDTMA to ODTMA). The fact that samples with higher actual amount of loaded surfactant present the maximum NO_3^- removal

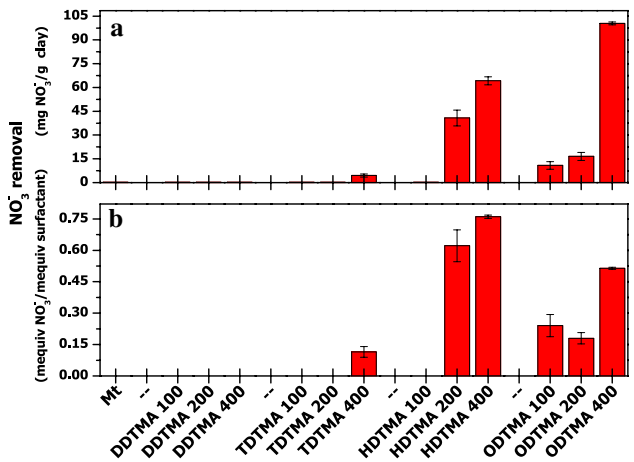

Fig. 1 NO_3^- removal by indicated samples (C_i = 100 mg L^{-1} NO_3^-, pH = 5.4 and solid/liquid ratio = 2 g L^{-1}). **a** mg NO_3^- related to g clay and **b** mequiv. NO_3^- related to mequiv. of actual surfactant

Table 1 Actual amounts of surfactant loaded as % CEC for all OMt samples

Initial amount of surfactant (%CEC)	Actual amount of surfactant loaded (%CEC)			
	DDTMA	TDTMA	HDTMA	ODTMA
100	67.9	72.4	81.7	88.5
200	69.1	76.7	128.2	179.7
400	101.0	107.0	165.1	379.5

values was indicative of the importance of the ammonium head content in NO_3^- removal [3]. This behaviour was also suggested by the higher values of NO_3^- adsorbed obtained in this work (40.7 mg and 64.2 mg NO_3^- per gram of clay, respectively) with respect to those obtained by Xi et al. (2010) (12.83 mg and 14.76 mg NO_3^- ions per gram clay) for HDTMA-200 and HDTMA-400 samples, where the lower CEC (0.667 mequiv. g^{-1}) reported for that raw Mt sample would be responsible for the lower NO_3^- uptake.

Figure 1b shows the NO_3^- retained normalized with respect to the mequiv. of the actual surfactant loaded for each OMt synthetized, in order to take into account the surfactant influence in the NO_3^-retention. The actual amount of the surfactant adsorbed on the Mt surface was determined in the following sections and listed in Table 1. For TDTMA and HDTMA loaded Mt, NO_3^- retention was significant when the actual amount of surfactant was greater than 100% CEC. However, for ODTMA loaded Mt the higher amount of NO_3^- attained seemed to be related to the actual surfactant content, despite it not reach 100% CEC (Table 1). These different behaviours could indicate that not only the amount of surfactant but also different surface sites (as will be analysed in the following sections: XRD and zeta potential) would be related to NO_3^- adsorption.

3.2 Thermogravimetric analysis

Several studies were carried out to understand the thermal behaviour of OMt exchanged with quaternary alkylammonium salts [38–42]. From these studies, three stages of mass loss were reported. The first stage (25–150 °C) is related to the physisorbed water loss. The second stage (150–550 °C) is associated with the organic matter oxidation and its loss as CO_2 and NO_2. Finally, the third stage (550–800 °C) comprises the dehydroxylation of the clay together with part of the organic matter that was not oxidized in the second stage.

From the mass loss in the region where organic molecules are broken down (150–800 °C), the actual surfactant loading was calculated. Table 1 lists the actual amounts of surfactant loaded as % CEC for all OMt samples.

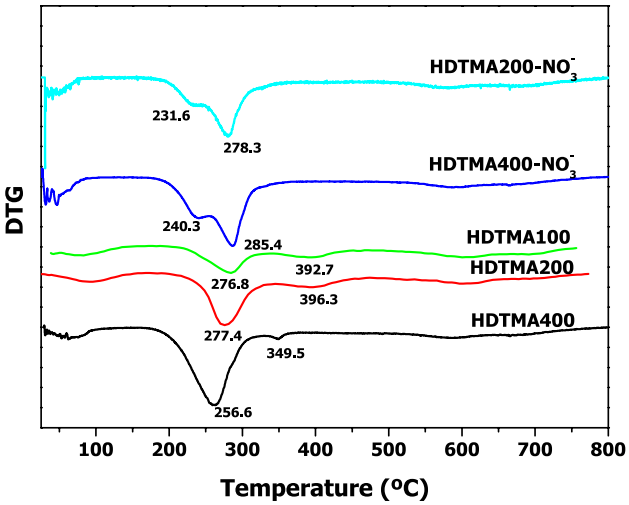

Fig. 2 DTG curves of HDTMA samples before and after NO_3^- adsorption

Table 1 shows dissimilar differences between the initial and actual amount of each surfactant loaded in the respective OMt samples, pointing out some dependence on the chain length of the surfactant employed. While for the short-chain surfactants (DDTMA and TDTMA) only when 400% CEC of the initial surfactant amount was added an actual 100% CEC value was reached, for long-chain surfactants (HDTMA and ODTMA) with 200% incorporated an actual amount higher than 100% CEC was already reached. To understand why, despite the same amount of initial surfactant added, the actual amount of surfactant loaded was lower when using short-chain than long-chain surfactants (Table 1), two different behaviours originated from the surfactant chain length should be considered. The first one is related to changes in the volume of the hydrophobic tail, and hence in the packing density, which are produced by the different surfactant chain lengths, generating diverse electrostatic interactions between the adsorbed ionic surfactants [43]. Açışlı et al. [32] assigned the electrostatic interactions mainly to hydrophobic interactions, which are smaller between the tails of relatively short-chain molecules than long ones. The second one is associated with the surfactant diffusion into the solution phase, or desorption, which is also driven by the strength of the hydrophobic interactions.

The modification of the DTG graphs, before and after NO_3^- retention for OMt samples, was exemplified by using HDTMA-Mt sample (Fig. 2). In HDTMA100, -200 and -400 samples two DTG peaks (at around 270 and 390 °C) associated with the decomposition temperature of the loaded surfactant were observed. These peaks were assigned previously [44] to two different interactions or association mechanisms between the Mt surface and the

surfactant. The first peak at around 270 °C was related to hydrophobic or van der Waals interactions, whereas the second one above 340 °C was attributed to a stronger interaction such as a cation exchange process. When the surfactant concentration is lower than 100% CEC, the organic cations are mainly adhered to the Mt surface sites via a cation exchange process. While at higher surfactant concentrations loaded (> 100% CEC) organic molecules attached to the external surface are related to hydrophobic interactions with other chains of the surfactant. These hydrophobic interactions decrease the de-surfactant temperature when the surfactant amount and packing density increased. These are due to the decrease of hydrophobic strength among the molecules [45].

The important temperature decrease for both peaks (more than 20 °C and 43 °C for low and high temperature peaks, respectively) and the relative intensity increase of the lower temperature peak (256.6 °C) found for HDTMA400 (Fig. 2) with respect to HDTMA100 sample corroborated the increase of hydrophobic interactions in the first sample, in agreement with data of our previous work [45].

For samples with adsorbed NO_3^-, the DTG peak assigned to the cationic interactions disappeared, while the one related to the hydrophobic interactions shifted to lower temperature, 278.3 °C and 285.4 °C for HDTMA200-NO_3^- and HDTMA400-NO_3^- samples, respectively (Fig. 2). The presence of new peaks at 231.6 and 240.3 °C could be assigned to some NO_3^- interaction with the HDTMA polar group adsorbed at the external surface probably through electrostatic interactions.

3.3 FTIR spectroscopy analysis

As an example, the identification of the NO_3^- retained by the OMt samples was followed by FTIR analysis of HDTMA loaded samples before and after NO_3^- retention, and is shown in Fig. 3.

The typical bands corresponding to the Mt structural groups νOH, νSiO, δAlAlOH, δAlOSi, and δSiOSi at 3632, 1040, 916, 521 and 461 cm^{-1} [18], respectively, can be identified irrespective of the loaded surfactant, while that at 1625 cm^{-1}, corresponding to water molecule deformation, shifted to 1639 cm^{-1} due to organic cation adsorption [46]. Besides these bands, for HDTMA loaded samples two intense absorption bands appeared at around 2920 and 2851 cm^{-1} corresponding to the asymmetric [ν_{as} (CH_2)] and symmetric [ν_s (CH_2)] stretching vibration of CH_2- groups (Fig. 3). The surfactant loading increase, irrespective of the surfactant employed (Figs. not shown), produces a shift towards a lower wavenumber range [47–49]. This shift was assigned to the sensitivity to the gauche/trans conformer ratio of the alkyl chains, which reflects the packing density increase of the alkyl chains with their length. This conclusion is consistent with the previous one based on the TG analysis (Table 1).

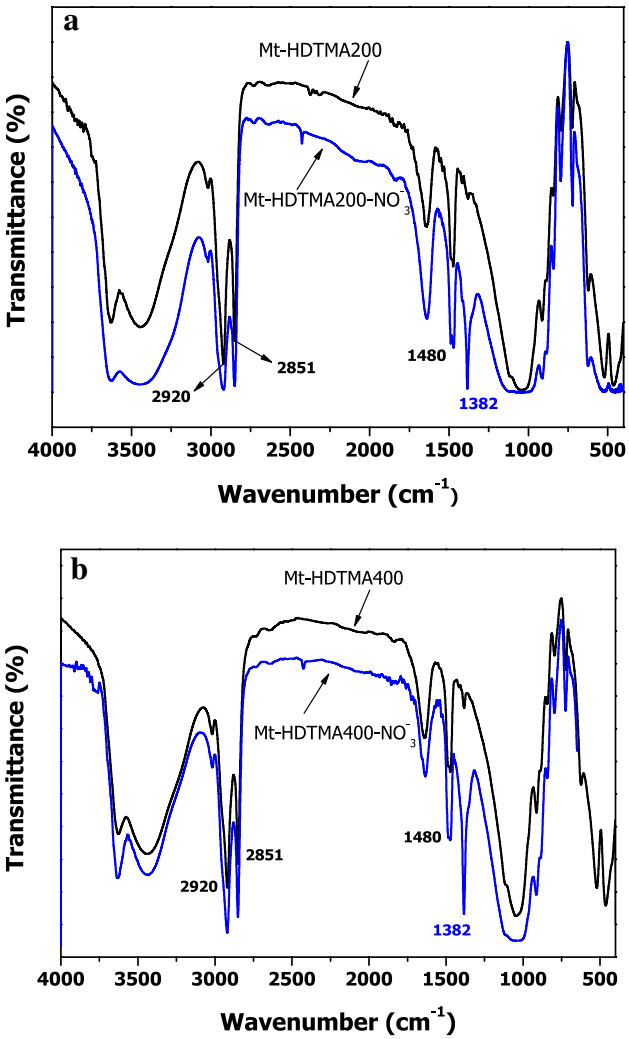

Fig. 3 FTIR spectra of HDTMA samples before and after NO_3^- adsorption

The band at around 1480 cm^{-1} was assigned to the bending vibration of the alkyl chains that remained at the same wavenumber irrespective of the surfactant loading.

The band at 1382 cm^{-1} was assigned to asymmetric stretching vibration of the nitrate ion [50], which was overlapped with that corresponding to the vibration of tetra-coordinated silicon in the Mt structure [51]. Despite the screening effect of the tetra-coordinated silicon band, its intensity increase could be correlated with nitrate adsorption (Fig. 3), in agreement with the results found for NO_3^- adsorbed on different materials [13, 51].

3.4 XRD results

The changes in the thickness of the interlayer can be evidenced by the shifts in 2 theta of the peak corresponding to the d001 value of the Mt sample. These shifts of basal space allow following the interlayer inorganic cations (Na^+, K^+ and Ca^{2+}) exchange by the respective cationic surfactant. A previous XRD spectrum of raw Mt [52] exhibited a diffraction peak at 6.95° (basal space: 1.27 nm) that indicated a typical smectite peak for pure montmorillonite [53], and the structural formula previously evaluated specified that it is Na-montmorillonite [36].

For the OMt samples, the cation exchange by the respective surfactants generated an increasing enlargement of raw Mt basal space with the chain length increase of the surfactant from 1.66 to 1.85 nm (Fig. 1), depending on the uptake and orientation in interlayer galleries of the organic cations, as was previously reported [39, 54]. The interlayer space thicknesses of OMt samples, determined from the difference between the basal space and that of dehydrated Mt (0.97 nm) [55], were in the range 0.69–0.95 nm corresponding to a bilayer arrangement. The ODTMA400 sample attained the highest interlayer space thickness of 1.05 nm corresponding to a pseudo-trilayer arrangement of the surfactant [56]. Within each surfactant, the surfactant loading increase also produced a different widening of the interlayer, which was assigned to the increase of the surfactant packing density, in accordance with FTIR analysis.

The samples HDTMA200, 400 and ODTMA100–400, after NO_3^- uptake, showed a slight basal space increase (Fig. 4), which could indicate the anion entrance into the interlayer space of montmorillonite by a synergic effect with cationic surfactants, as was found between $HDTMA^+$ and the anionic surfactant sodium dodecyl sulfonate [57].

3.5 Zeta potential

The variation of the electric charge on the external surface of the Mt and OMt samples without and with NO_3^- can be measured by modifications in the zeta potential value. The zeta potential of Mt sample presents the well-known negative electric surface charge, with a very small effect of pH and ionic strength [34], and the zeta potential value around − 37 mV in the pH range of 2–10 [20].

It is worth noting that when Mt is loaded with surfactants to obtain OMt samples, a decrease of the negative zeta potential value was observed (Fig. 5) [18, 31, 32].

The different chain length of charged surfactants markedly modifies the sign of the zeta potential obtained for the corresponding OMt (Fig. 5). For OMt samples loaded with DDTMA (with 67.9–101% CEC, Table 1) the value of the zeta potential remained negative, while for OMt

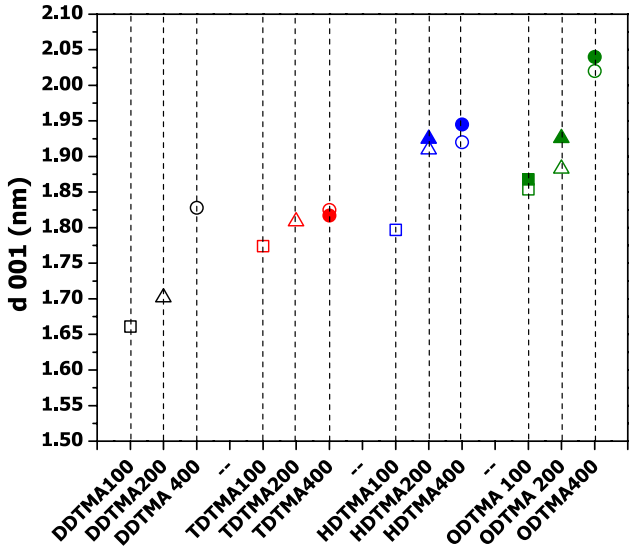

Fig. 4 The d001 values for indicated samples. Symbols indicate: (empty) without and (full) with NO_3

samples loaded with the longer chain surfactant (ODTMA) (with contents between 88.5 and 379.5% CEC, Table 1) the zeta potential sign reversed to positive. The surfactants with intermediate chain length (TDTMA and HDTMA) showed negative zeta potential values for surfactant loading < 100% CEC, while the zeta potential sign reversed when loading was > 100% CEC. Particularly, for TDTMA-200 sample with actual 76.7% CEC loaded, the pH dependence on the zeta potential sign led to the determination of an IEP at around pH = 5.0, which indicated that variable charges dominate the surface charge behaviour [58].

The negative zeta potential values attained for OMt samples loaded with DDTMA and < 100% CEC for TDTMA and HDTMA validate the null NO_3^- adsorption obtained (Fig. 1a).

In general, the decrease of the positive zeta potential values after NO_3^- adsorption for long-chain surfactant loaded samples and also with TDMA loaded with 107% CEC agrees with the NO_3^- adsorption found (Fig. 1a). This behaviour was also reported by Açışlı et al. (2017) and assigned to the dominant role, in the clay adsorption process, of the mutual interactions of surfactants with longer chain length with respect to the surface charge of the clay.

However, two different mechanisms could be involved for NO_3^- retention at these OMt surfaces: (a) NO_3^- coating of the external surface, as happened for magnetite in our previous work [52], and/or (b) ion pair interactions between the surfactant positive polar group and NO_3^-. The increase of the relationship NO_3^-/surfactant (Fig. 1b) found for long-chain surfactants could mainly be assigned to the formation of ion pairs, while for ODTMA-100 sample (with actual surfactant loading of 88.5% CEC) the NO_3^- entrance

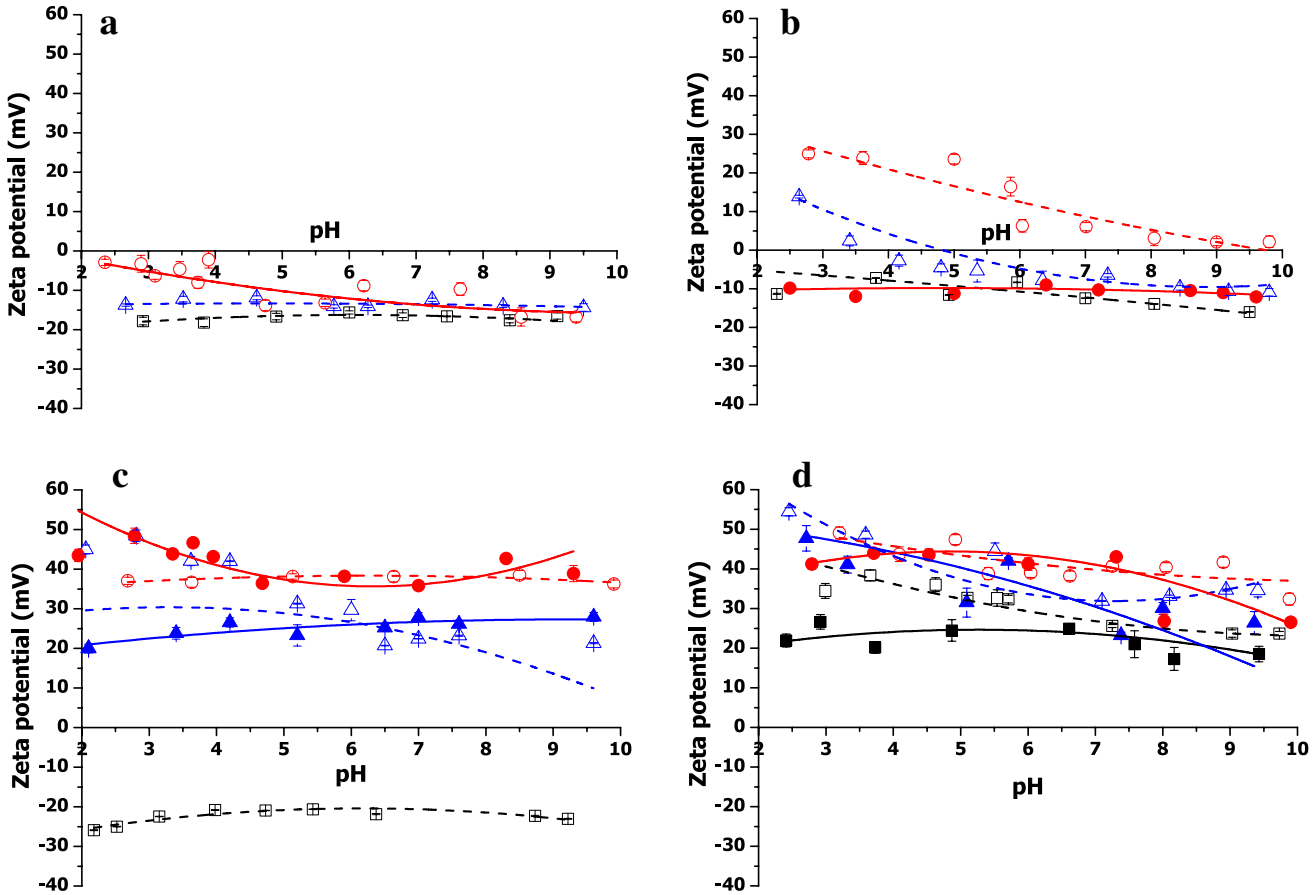

Fig. 5 Zeta potential versus pH curves for **a** DDTMA, **b** TDTMA, **c** HDTMA and **d** ODTMA samples. Symbols indicate: (open square) 100; (open triangle) 200 and (open circle) 400% initial loaded surfactant. Symbols indicate: (empty) without and (full) with NO_3^-

to the Mt interlayer (as indicated by the XRD analysis) must not be neglected and could originate the higher value of the relationship NO_3^-/surfactant obtained with respect to the higher ODTMA loaded sample (with actual surfactant loading of 179.7% CEC).

4 Conclusions

The NO_3^- adsorption inefficiency found for raw Mt was reversed by OMt samples prepared with different long-chain length surfactants (ODTMA and HDTMA) and loaded with 100%, 200% or 400% CEC. Among the OMt evaluated as adsorbent, a higher NO_3^- adsorption was found for samples with 400% CEC initial surfactant loading amount, attaining a maximal value of 100 and 64 mg NO_3^- ions per gram of OMt for ODTMA400 and HDTMA400 samples, respectively. The thermogravimetric analysis of OMt samples allowed the determination of the actual amount of loaded surfactant. In addition, in a temperature range of 230–240 °C a new peak appeared, which could be assigned to the NO_3^- interactions with the surfactant on the external surface. The XRD and zeta potential measurements pointed to the existence of synergic effects between the NO_3^- and long-chain surfactants generating the thickness increase of the interlayer, while the ion pair interactions between the NO_3^- and the positive polar group of long-chain surfactants were the promoters of the loss of positive external surface charges.

Acknowledgements Financial support of the Argentine Ministry of Science, ANPCyT, PICT 2010/585, 2016/1391 and PME8-2003 for the purchase of the SPECS multi-technique analysis instrument, CONICET PIP 0276 and 1178, and UNLP (Project I172, X633 and X700) are gratefully acknowledged. M.A.J, M.L.C, M.A.F. and R.M.T.S. are members of the National Council of Scientific and Technological Research (CONICET) and F.M. Flores acknowledges CONICET fellowships. Authors thank the technical assistance of Gabriela Garcia from INTI CAUCHO to perform the FTIR spectra.

Compliance with ethical standards

Conflict of interest On behalf of all authors, the corresponding author states that there is no conflict of interest.

References

1. Haber F, Le Rossignol R (1910) Production of ammonia. US Patent
2. Costa AO, Ferreira LS, Passos FB, Maia MP, Peixoto FC (2012) Microkinetic modeling of the hydrogenation of nitrate in water on Pd–Sn/Al_2O_3 catalyst. Appl Catal A Gen 445–446:26–34. https://doi.org/10.1016/j.apcata.2012.07.043
3. Loganathan P, Vigneswaran S, Kandasamy J (2013) Enhanced removal of nitrate from water using surface modification of adsorbents—a review. J Environ Manag 131:363–374. https://doi.org/10.1016/j.jenvman.2013.09.034
4. Teimouri A, Nasab SG, Vahdatpoor N, Habibollahi S, Salavati H, Chermahini AN (2016) Chitosan/Zeolite Y/Nano ZrO_2 nanocomposite as an adsorbent for the removal of nitrate from the aqueous solution. Int J Biol Macromol 93:254–266. https://doi.org/10.1016/j.ijbiomac.2016.05.089
5. EPA (2009) National Primary Drinking Water Regulations. https://www.epa.gov/sites/production/files/2016-06/documents/npwdr_complete_table.pdf. Accesed 19 Mar 2019
6. WHO (2011) Nitrate and nitrite in drinking-water. World Health Organization web page. www.who.int/water_sanitation_health/dwq/chemicals/nitratenitrite2ndadd.pdf. Accesed 19 Mar 2019
7. Zhai Y, Zhao X, Teng Y, Li X, Zhang J, Wu J, Zuo R (2017) Groundwater nitrate pollution and human health risk assessment by using HHRA model in an agricultural area, NE China. Ecotoxicol Environ Saf 137:130–142. https://doi.org/10.1016/j.ecoenv.2016.11.010
8. Islam M, Patel R (2010) Synthesis and physicochemical characterization of Zn/Al chloride layered double hydroxide and evaluation of its nitrate removal efficiency. Desalination 256:120–128. https://doi.org/10.1016/j.desal.2010.02.003
9. Palko JW, Oyarzun DI, Ha B, Stadermann M, Santiago JG (2018) Nitrate removal from water using electrostatic regeneration of functionalized adsorbent. Chem Eng J 334:1289–1296. https://doi.org/10.1016/j.cej.2017.10.161
10. Rezvani F, Sarrafzadeh MH, Ebrahimi S, Oh HM (2019) Nitrate removal from drinking water with a focus on biological methods: a review. Environ Sci Pollut Res 26:1124–1141. https://doi.org/10.1007/s11356-017-9185-0
11. Rezvani P, Taghizadeh MM (2018) On using clay and nanoclay ceramic granules in reducing lead, arsenic, nitrate, and turbidity from water. Appl Water Sci 8:131. https://doi.org/10.1007/s13201-018-0779-6
12. Bhatnagar A, Sillanpää M (2011) A review of emerging adsorbents for nitrate removal from water. Chem Eng J 168:493–504. https://doi.org/10.1016/j.cej.2011.01.103
13. Wu Y, Wang Y, Wang J, Xu S, Yu L, Philippe C, Wintgens T (2016) Nitrate removal from water by new polymeric adsorbent modified with amino and quaternary ammonium groups: batch and column adsorption study. J Taiwan Inst Chem Eng 66:191–199. https://doi.org/10.1016/j.jtice.2016.06.019
14. Nunell GV, Fernandez ME, Bonelli PR, Cukierman AL (2015) Nitrate uptake from water by means of tailored adsorbents. Water Air Soil Pollut 226:278. https://doi.org/10.1007/s11270-015-2546-8
15. Islam M, Patel R (2011) Physicochemical characterization and adsorption behavior of Ca/Al chloride hydrotalcite-like compound towards removal of nitrate. J Hazard Mater 190:659–668. https://doi.org/10.1016/j.jhazmat.2011.03.094
16. Renault F, Morin-Grini N, Badot PM, Crini G (2011) Non-conventional sorbents for dyes removal. In: Badot PM, Crini G (eds) Sorption processes and pollution: conventional and non-conventional sorbents for pollutant removal from wastemasters. Presses Universitaires de Franche-Comté, Besançon, pp 187–205
17. Flores FM, Undabeytia T, Morillo E, Torres Sánchez RM (2017) Technological applications of organo-montmorillonites in the removal of pyrimethanil from water: adsorption/desorption and flocculation studies. Environ Sci Pollut Res 24:14463–14476. https://doi.org/10.1007/s11356-017-9016-3
18. Gamba M, Flores FM, Madejová J, Sánchez RMT (2015) Comparison of imazalil removal onto montmorillonite and nano-montmorillonite and adsorption surface sites involved: an approach for agricultural wastewater treatment. Ind Eng Chem Res 54:1529–1538. https://doi.org/10.1021/ie5035804
19. Gamba M, Lázaro-Martínez JM, Olivelli MS, Yarza F, Vega D, Curutchet G, Torres Sánchez RM (2019) Kinetic and equilibrium adsorption of two post-harvest fungicides onto copper-exchanged montmorillonite: synergic and antagonistic effects of both fungicides' presence. Environ Sci Pollut Res 26:2421–2434. https://doi.org/10.1007/s11356-018-3638-y
20. Maqueda C, Dos Santos Afonso M, Morillo E, Torres Sánchez RM, Perez-Sayago M, Undabeytia T (2013) Adsorption of diuron on mechanically and thermally treated montmorillonite and sepiolite. Appl Clay Sci 72:175–183. https://doi.org/10.1016/j.clay.2012.10.017
21. Flores FM, Loveira EL, Yarza F, Candal R, Sánchez RMT (2017) Benzalkonium chloride surface adsorption and release by two montmorillonites and their modified organomontmorillonites. Water Air Soil Pollut 228:42. https://doi.org/10.1007/s11270-016-3223-2
22. Zhu R, Chen Q, Zhou Q, Xi Y, Zhu J, He H (2016) Adsorbents based on montmorillonite for contaminant removal from water: a review. Appl Clay Sci 123:239–258. https://doi.org/10.1016/j.clay.2015.12.024
23. Gammoudi S, Frini-Srasra N, Srasra E (2013) Preparation, characterization of organosmectites and fluoride ion removal. Int J Miner Process 125:10–17. https://doi.org/10.1016/j.minpro.2013.09.003
24. Gammoudi S, Frini-Srasra N, Srasra E (2012) Nitrate sorption by organosmectites. Eng Geol 124:119–129. https://doi.org/10.1016/j.enggeo.2011.10.009
25. Lee YC, Kim EJ, Shin HJ, Choi M, Yang JW (2012) Removal of F^-, NO_3^-, and PO_4^{3-} ions from aqueous solution by aminoclays. J Ind Eng Chem 18:871–875. https://doi.org/10.1016/j.jiec.2011.12.008
26. Xi Y, Mallavarapu M, Naidu R (2010) Preparation, characterization of surfactants modified clay minerals and nitrate adsorption. Appl Clay Sci 48:92–96. https://doi.org/10.1016/j.clay.2009.11.047
27. Uddin MK (2017) A review on the adsorption of heavy metals by clay minerals, with special focus on the past decade. Chem Eng J 308:438–462. https://doi.org/10.1016/j.cej.2016.09.029
28. Dutta A, Singh N (2015) Surfactant-modified bentonite clays: preparation, characterization, and atrazine removal. Environ Sci Pollut Res 22:3876–3885. https://doi.org/10.1007/s11356-014-3656-3
29. He H, Frost RL, Bostrom T, Yuan P, Duong L, Yang D, Xi Y, Kloprogge JT (2006) Changes in the morphology of organoclays with $HDTMA^+$ surfactant loading. Appl Clay Sci 31:262–271. https://doi.org/10.1016/j.clay.2005.10.011
30. Praus P, Turicová M, Študentová S, Ritz M (2006) Study of cetyltrimethylammonium and cetylpyridinium adsorption on montmorillonite. J Colloid Interface Sci 304:29–36. https://doi.org/10.1016/j.jcis.2006.08.038
31. Bianchi AE, Fernández M, Pantanetti M, Viña R, Torriani I, Sánchez RMT, Punte G (2013) $ODTMA^+$ and $HDTMA^+$ organomontmorillonites characterization: new insight by WAXS, SAXS and surface charge. Appl Clay Sci 83–84:280–285. https://doi.org/10.1016/j.clay.2013.08.032

32. Açışlı Ö, Karaca S, Gürses A (2017) Investigation of the alkyl chain lengths of surfactants on their adsorption by montmorillonite (Mt) from aqueous solutions. Appl Clay Sci 142:90–99. https://doi.org/10.1016/j.clay.2016.12.009
33. Jaber M, Komarneni S, Zhou CH (2013) Synthesis of clay minerals. In: Lagaly G, Bergaya F (eds) Handbook of clay science. Elsevier, Amsterdam, pp 223–241
34. Zadaka D, Radian A, Mishael YG (2010) Applying zeta potential measurements to characterize the adsorption on montmorillonite of organic cations as monomers, micelles, or polymers. J Colloid Interface Sci 352:171–177. https://doi.org/10.1016/j.jcis.2010.08.010
35. Haggerty GM, Bowman RS (1994) Sorption of chromate and other inorganic anions by organo-zeolite. Environ Sci Technol 28:452–458. https://doi.org/10.1021/es00052a017
36. Magnoli AP, Tallone L, Rosa CAR, Dalcero AM, Chiacchiera SM, Torres Sanchez RM (2008) Commercial bentonites as detoxifier of broiler feed contaminated with aflatoxin. Appl Clay Sci 40:63–71. https://doi.org/10.1016/j.clay.2007.07.007
37. Xie W, Gao Z, Pan WP, Hunter D, Singh A, Vaia R (2001) Thermal degradation chemistry of alkyl quaternary ammonium montmorillonite. Chem Mater 13:2979–2990. https://doi.org/10.1021/cm010305s
38. Ganguly S, Dana K, Mukhopadhyay TK, Ghatak S (2011) Thermal degradation of alkyl triphenyl phosphonium intercalated montmorillonites: an isothermal kinetic study. J Therm Anal Calorim 105:199–209. https://doi.org/10.1007/s10973-011-1356-5
39. He H, Ma Y, Zhu J, Yuan P, Qing Y (2010) Organoclays prepared from montmorillonites with different cation exchange capacity and surfactant configuration. Appl Clay Sci 48:67–72. https://doi.org/10.1016/j.clay.2009.11.024
40. Keidar O, Lapides I, Shoval S, Yariv S (2015) Thermogravimetry and differential thermal analysis of montmorillonite treated with 1,4-diaminoanthraquinone. J Therm Anal Calorim 120:33–43. https://doi.org/10.1007/s10973-014-4310-5
41. Yariv S (2004) The role of charcoal on DTA curves of organo-clay complexes: an overview. Appl Clay Sci 24:225–236. https://doi.org/10.1016/j.clay.2003.04.002
42. Yariv S, Borisover M, Lapides I (2011) Few introducing comments on the thermal analysis of organoclays. J Therm Anal Calorim 105:897–906. https://doi.org/10.1007/s10973-010-1221-y
43. Nagarajan R (2002) Molecular packing parameter and surfactant self-assembly: the neglected role of the surfactant tail. Langmuir 18:31–38. https://doi.org/10.1021/la010831y
44. Naranjo PM, Sham EL, Castellón ER, Torres Sánchez RM, Farfán Torres EM (2013) Identification and quantification of the interaction mechanisms between the cationic surfactant HDTMA-Br and montmorillonite. Clays Clay Miner 61:98–106. https://doi.org/10.1346/ccmn.2013.0610208
45. Fernández Solarte AM, Villarroel-Rocha J, Morantes CF, Montes ML, Sapag K, Curutchet G, Torres Sánchez RM (2018) Insight into surface and structural changes of montmorillonite and organomontmorillonites loaded with Ag. C R Chim. https://doi.org/10.1016/j.crci.2018.09.006
46. Madejová J (2003) FTIR techniques in clay mineral studies. Vib Spectrosc 31:1–10. https://doi.org/10.1016/s0924-2031(02)00065-6
47. Frost RL, Zhou Q, He H, Xi Y (2008) An infrared study of adsorption of para-nitrophenol on mono-, di- and tri-alkyl surfactant intercalated organoclays. Spectrochimica Acta Part A Mol Biomol Spectrosc 69:239–244. https://doi.org/10.1016/j.saa.2007.02.023
48. He H, Frost LR, Zhu J (2004) Infrared study of $HDTMA^+$ intercalated montmorillonite. Spectrochim Acta Part A Mol Biomol Spectrosc 60:2853–2859. https://doi.org/10.1016/j.saa.2003.09.028
49. Zhu J, Wang T, Zhu R, Ge F, Wei J, Yuan P, He H (2011) Novel polymer/surfactant modified montmorillonite hybrids and the implications for the treatment of hydrophobic organic compounds in wastewaters. Appl Clay Sci 51:317–322. https://doi.org/10.1016/j.clay.2010.12.016
50. Gadsden JA (1975) Infrared spectra of minerals and related inorganic compounds. Butterworths, London
51. Carvalho A, Pires J, Veloso P, Machado M, Brotas de Carvalho M, Rocha J (2003) Nitrate occlusion studies in Y zeolite and in a clay pillared with aluminium oxide. Microporous Mesoporous Mater 58:163–173. https://doi.org/10.1016/s1387-1811(02)00625-x
52. Barraqué F, Montes ML, Fernández MA, Mercader RC, Candal RJ, Torres Sánchez RM (2018) Synthesis and characterization of magnetic-montmorillonite and magnetic-organo-montmorillonite: surface sites involved on cobalt sorption. J Magn Magn Mater 466:376–384. https://doi.org/10.1016/j.jmmm.2018.07.052
53. Ejder-Korucu M, Gürses A, Karaca S (2016) Poly(ethylene oxide)/clay nanaocomposites: thermal and mechanical properties. Appl Surf Sci 378:1–7. https://doi.org/10.1016/j.apsusc.2016.03.159
54. Schampera B, Tunega D, Šolc R, Woche SK, Mikutta R, Wirth R, Dultz S, Guggenberger G (2016) External surface structure of organoclays analyzed by transmission electron microscopy and X-ray photoelectron spectroscopy in combination with molecular dynamics simulations. J Colloid Interface Sci 478:188–200. https://doi.org/10.1016/j.jcis.2016.06.008
55. Emmerich K, Plötze M, Kahr G (2001) Reversible collapse and Mg^{2+} release of de- and rehydroxylated homoionic cis-vacant montmorillonites. Appl Clay Sci 19:143–154. https://doi.org/10.1016/s0169-1317(01)00049-7
56. Zhu J, He H, Guo J, Yang D, Xie X (2003) Arrangement models of alkylammonium cations in the interlayer of $HDTMA^+$ pillared montmorillonites. Chin Sci Bull 48:368–372. https://doi.org/10.1360/03tb9078
57. Fu M, Zhang Z, Wu L, Zhuang G, Zhang S, Yuan J, Liao L (2016) Investigation on the co-modification process of montmorillonite by anionic and cationic surfactants. Appl Clay Sci 132–133:694–701. https://doi.org/10.1016/j.clay.2016.08.025
58. Pecini EM, Avena MJ (2013) Measuring the isoelectric point of the edges of clay mineral particles: the case of montmorillonite. Langmuir 29:14926–14934. https://doi.org/10.1021/la403384g